International Journal of Biological Macromolecules 225 (2023) 135–148

Contents lists available at ScienceDirect

International Journal of Biological Macromolecules

journal homepage: www.elsevier.com/locate/ijbiomac

Rationally designed antifungal protein chimeras reveal new insights into structure-activity relationship

Moisés Giner-Llorca [a,1], Francisca Gallego del Sol [b,1], Jose F. Marcos [a], Alberto Marina [b,*], Paloma Manzanares [a,**]

[a] Food Biotechnology Department, Instituto de Agroquímica y Tecnología de Alimentos (IATA), Consejo Superior de Investigaciones Científicas (CSIC), Catedrático Agustín Escardino Benlloch 7, 46980 Paterna, Valencia, Spain
[b] Instituto de Biomedicina de Valencia (IBV), CSIC and CIBER de Enfermedades Raras (CIBERER), Jaume Roig 11, 46010, Valencia, Spain

ARTICLE INFO

Keywords:
Antifungal proteins
3D structure
Crystallography
Rational design
Chimeras
Mannoproteins
Phospholipids

ABSTRACT

Antifungal proteins (AFPs) are promising antimicrobial compounds that represent a feasible alternative to fungicides. *Penicillium expansum* encodes three phylogenetically distinct AFPs (PeAfpA, PeAfpB and PeAfpC) which show different antifungal profiles and fruit protection effects. To gain knowledge about the structural determinants governing their activity, we solved the crystal structure of PeAfpB and rationally designed five PeAfpA::PeAfpB chimeras (chPeAFPV1-V5). Chimeras showed significant differences in their antifungal activity. chPeAFPV1 and chPeAFPV2 improved the parental PeAfpB potency, and it was very similar to that of PeAfpA. chPeAFPV4 and chPeAFPV5 showed an intermediate profile of activity compared to the parental proteins while chPeAFPV3 was inactive towards most of the fungi tested. Structural analysis of the chimeras evidenced an identical scaffold to PeAfpB, suggesting that the differences in activity are due to the contributions of specific residues and not to induced conformational changes or structural rearrangements. Results suggest that mannoproteins determine protein interaction with the cell wall and its antifungal activity while there is not a direct correlation between binding to membrane phospholipids and activity. This work provides new insights about the relevance of sequence motifs and the feasibility of modifying protein specificity, opening the door to the rational design of chimeras with biotechnological applicability.

1. Introduction

Antifungal proteins (AFPs) secreted by filamentous ascomycetes are small, cationic cysteine-rich proteins (CRPs) that exhibit potent antifungal activity against important human, animal, plant and foodborne pathogenic fungi [1–4]. AFPs contain six to eight cysteine residues that form three or four intramolecular disulfide bonds stabilizing an antiparallel β-sheet structure with surface-exposed loops. This compact tertiary structure makes AFPs highly stable against adverse biochemical and biophysical conditions such as pH, temperature and proteolysis [5]. AFPs contain a conserved γ-core motif which consists of the consensus amino acid sequence $GXCX_{3-9}C$ [6] preceded by an N-terminal sequence that includes the signal peptide (SP) involved in AFP secretion to the extracellular space and a pro-sequence (SP-pro sequence) that has been predicted to inactivate the protein until cleavage [7].

Fungi have a complex repertoire of phylogenetically distinct AFP and AFP-like sequences [8]. To date >50 members have been identified in the AFP family. Based on phylogenetic clustering but also on sequence alignment, cysteine pattern, intron position and Pfam domain identification, we proposed the classification of fungal AFPs into three classes: A, B and C [8]. Notably, some fungal genomes encode more than one AFP each belonging to a different phylogenetic class [8]. Based on their properties and natural diversity, AFPs are attractive antifungal agents or lead compounds for the next generation of fungicides to fight infections that severely threaten human health and food safety. Furthermore, exploitation of AFPs is feasible, since safe and efficient fungus- or plant-based biofactories have been developed for their production [9–11].

Current knowledge about the killing mechanisms of AFPs is still limited, which hampers their potential improvement by rational design and applicability. Killing mechanisms are mainly based on a cell-

* Correspondence to: A. Marina, IBV-CSIC, Jaume Roig 11, 46010, Valencia, Spain.
** Correspondence to: P. Manzanares, IATA-CSIC, Catedrático Agustín Escardino Benlloch 7, Paterna 46980, Valencia, Spain.
E-mail addresses: amarina@ibv.csic.es (A. Marina), pmanz@iata.csic.es (P. Manzanares).
[1] Contributed equally to this work.

https://doi.org/10.1016/j.ijbiomac.2022.11.280
Received 27 September 2022; Received in revised form 25 November 2022; Accepted 27 November 2022
Available online 29 November 2022

penetrating mode of action as described for *Penicillium chrysogenum* AFPs [12–14] and *Penicillium digitatum* PdAfpB [15], or the disruption of plasma membrane integrity as reported for *Aspergillus giganteus* AFP [16–18] and *Neosartorya fischeri* NFAP2 [19]. Regardless the mode of action, mechanistic studies have shown that AFPs act through multiple targets, including components of fungal cell wall [15,20,21], plasma membrane lipids [18,22] and intracellular processes [14,15,23,24].

Rational design of new-to-nature AFPs with improved properties requires a comprehensive understanding of the structural domains that account for the antifungal activity. Several strategies have been described to map the antifungal domains of AFPs. Targeted amino acid substitutions in the *P. chrysogenum* PAF sequence revealed the importance of a negatively charged residue for the protein structure and mechanistic function [25], or the significant influence of the γ-core motif on the PAF antifungal efficacy [26]. Different substitutions in *N. fischeri* NFAP sequence allowed the identification of the structural determinants for folding, stability and activity [27]. Rational design of Cys-containing peptides based on the primary sequence of PdAfpB as well as PdAfpB chimeric proteins contributed to the mapping of antifungal motifs [28,29].

In previous works, we characterized the pattern of production and antifungal profiles of the three *P. expansum* AFPs, PeAfpA, PeAfpB and PeAfpC [30–32]. These studies underlined the high potency of PeAfpA against economically important phytopathogenic fungi and mycotoxin-producer fungi, dermatophytes and clinically relevant yeasts. PeAfpB, although less effective than PeAfpA, showed significant activity against most of the mycotoxigenic fungi tested, while PeAfpC was inactive against most of the fungi evaluated and only showed a powerful inhibition against *Byssochlamys* species [32]. PeAfpA protects against infections caused by *P. digitatum* in oranges, *P. expansum* in apples, and *Botrytis cinerea* in tomato plants and fruits [30,31], while PeAfpB showed a modest disease reduction in apples [30]. Despite the potential of PeAFPs as biofungicides, little is known about the structural determinants or molecular targets determining their antifungal activity. In the present study, we report the 3D structure of PeAfpB solved by X-ray crystallography and the rational design of five PeAfpB::PeAfpA chimeras (chPeAFPV1-V5). We have characterized the chimeras and identified the contributions of different PeAfpA motifs to the antifungal activity. Moreover, the role of protein mannosylation and membrane lipids in the mode of action of native PeAFPs and chimeras is investigated. Finally, the X-ray 3D structure of four chimeras are presented, confirming that AFPs of class A and B share a highly stable structural scaffold and opening the door to the rational design of variants with biotechnological applicability.

2. Materials and methods

2.1. Strains, media and culture conditions

P. chrysogenum Δ*paf* strain [33] was used for genetic transformation and recombinant protein production. For the antimicrobial assays, the following fungal strains were used: *P. expansum* CECT 20906 (CMP-1), *P. digitatum* CECT 20796 (PHI-26), *B. cinerea* CECT 20516, *B. spectabilis* CECT 2983, *Fusarium oxysporum* 4287, *Magnaporthe oryzae* PR9 and *Saccharomyces cerevisiae* BY4741. Filamentous fungi were cultured in Potato Dextrose Agar (PDA, Difco-BD Diagnostics, Sparks, MD, United States) plates at 25 °C for 5–10 days depending on the fungus. *S. cerevisiae* was grown in Yeast Extract Peptone Dextrose Agar (YPDA) plates at 30 °C for 2 days.

For fungal transformation, vectors were propagated in *Escherichia coli* JM109 grown at 37 °C in Luria Bertani (LB) medium supplemented with either 25 μg/mL chloramphenicol, 50 μg/mL kanamycin or 100 μg/mL spectinomycin depending on the vector. *Agrobacterium tumefaciens* AGL-1 strain was grown in LB supplemented with 20 μg/mL rifampicin at 28 °C. To analyze the growth of the *P. chrysogenum* transformant strains in solid media, 5 μL of conidial suspension (5×10^4 conida/mL) were placed on the center of PDA and *P. chrysogenum* minimal medium (PcMM) [11] plates, and the colony diameter was monitored daily from 3 to 7 days. For recombinant protein production, transformant strains were inoculated at 10^6 conidia/mL in PcMM at 25 °C and 150 rpm for 5 days.

2.2. Generation of molecular assemblies for genetic transformation of *P. chrysogenum*

All the genetic elements previously available or generated in this study are described in Table S1. All the molecular assemblies used to produce the recombinant proteins were generated with the Goldenbraid (GB)-based modular cloning platform FungalBraid (FB) [34,35]. The coding sequence for the *P. expansum afpB* gene (Pexp_A0A0A2K0J0) and chimeras were designed according to GB rules (https://gbcloning.upv.es) and provided by an external company (IDT, Integrated DNA Technologies) as synthetic genes (gBlocks™ gene fragments). Each single genetic element was ligated into the domestication entry vector pUPD2 through protocols described previously [34,35] to obtain FB173, FB174, FB175, FB176, FB177 and FB180 elements (Table S1). Positive *E. coli* clones were confirmed by routine PCR amplifications using external specific primers designed for pUPD2 vectors [34] (Table S2) and confirmed by Sanger sequencing. Multipartite assemblies to obtain the transcriptional units (TU) to drive the production of AFPs under the control of the *paf* promoter (P*paf*; FB029) and terminator (T*paf*; FB030) were generated (FB183-FB188; Table S1). Finally, binary assemblies used for fungal transformation (FB190, FB192, FB194, FB196, FB198 and FB200; Table S1) combine the TUs for the production of AFPs with the TU used as fungal positive selection marker (geneticin (*nptII*) FB009). Positive *E. coli* clones and correct assembly were confirmed by restriction and/or PCR analyses using combinations of the universal specific primers designed for pDGB3 vectors (Table S2) [34].

2.3. *A. tumefaciens* mediated transformation of *P. chrysogenum*

The *A. tumefaciens* AGL-1 strain was used for fungal transformation [36]. Binary assemblies generated for fungal transformation (FB190, FB192, FB194, FB196, FB198 and FB200) were introduced into *A. tumefaciens* AGL-1 strain by electroporation. *P. chrysogenum* Δ*paf* was genetically transformed through *A. tumefaciens*-mediated transformation (ATMT) as described [35,37]. *P. chrysogenum* transformants were selected in 25 μg/mL geneticin (G418) (Invivogen, San Diego, CA, USA). All transformants were confirmed by PCR (Table S2; Fig. S1) using genomic DNA isolated as described previously [38], and subsequently by 1 % agarose gel electrophoresis.

2.4. Production and purification of recombinant proteins

PeAfpA and PeAfpC were purified as previously described [31]. For PeAfpB and chimera production, *P. chrysogenum* transformants were grown in PcMM for 5 days at 25 °C and 150 rpm (final concentration 10^6 conidia/mL). PeAfpB and chimeras were purified from cell-free supernatants collected by centrifugation and dialyzed (3.5 kDa molecular weight cut-off; Thermo Scientific) against 20 mM sodium phosphate buffer pH 6.5. Dialyzed solutions were applied to an AKTA system (AKTA Pure 25 L, Cytiva Life Sciences) equipped with a 5 mL HiTrap Capto S cation exchange chromatography column (Cytiva Life Sciences). Protein was eluted with a linear NaCl gradient from 0 to 0.5 M in the same buffer. Protein containing fractions were pooled and dialyzed against Milli-Q water. Protein concentration was determined spectrophotometrically (A280) considering the molar extinction coefficient of each variant (Table 1). The purity was checked by SDS-PAGE [39]; samples in denaturing buffer containing 5.5 % β-mercaptoethanol were loaded into SDS-16 % polyacrylamide gels calibrated with prestained protein size-standard SeeBlue R (Thermo Fisher Scientific, Waltham, MA, United States) and Coomassie blue stained.

Table 1
Physicochemical properties of parental and chimeric antifungal proteins. Molecular mass (MM), ε_{280}, isoelectric point (pI) and grand average hydropathy (GRAVY) are theoretical measures obtained from ProtParam tool of the ExPASy Proteomics Server [74]. Net charge at pH 7 is a theoretical measure obtained from Protein Calculator v3.4 (http://protcalc.sourceforge.net).

Protein	aa	MM (kDa)	Ɛ280	pI	Net charge (pH 7)	GRAVY
PeAfpA	57	6.64	0.673	9.48	8.7	−1.08
PeAfpB	58	6.69	0.668	7.80	2.2	−1.47
chPeAFPV1	58	6.67	0.670	8.27	2.9	−1.48
chPeAFPV2	58	6.62	0.675	8.27	2.9	−1.33
chPeAFPV3	58	6.66	0.671	7.77	1.7	−1.53
chPeAFPV4	58	6.72	0.887	8.26	2.7	−1.46
chPeAFPV5	58	6.81	0.656	8.27	3.2	−1.60

2.5. Western blot analyses

Purified AFPs were separated in SDS-16 % polyacrylamide gels and transferred to Amersham Protran 0.20 μm NC nitrocellulose transfer membrane (Cytiva Life Sciences). Protein detection was accomplished using anti-PeAfpA antibody diluted 1:2500 or anti-PeAfpB antibody diluted 1:1500 [31]. As secondary antibody, 1:20,000 dilution of ECL NA934 horseradish peroxidase donkey anti-rabbit (Cytiva Life Sciences) was used, and chemiluminescent detection was performed with ECL-Select Western blotting detection reagent (Cytiva Life Sciences) using the Amersham Imager 680 (Cytiva Life Sciences). The experiments were repeated at least twice.

2.6. Liquid chromatography electrospray ionization tandem mass spectrometry (LC-ESI-MS/MS)

Analyses were performed in the proteomics facility at the National Center for Biotechnology of the Spanish National Research Council (CNB-CSIC). Samples from bands excised from SDS-PAGE gels were derivatized with propionic anhydride and automatically digested with trypsin in a 96-well plate using the OT-2 robot (Opentrons). The resulting mixtures were quantified by fluorimetry and ½ of each sample was injected into the chromatograph. Data acquisition was carried out by a combination of a 30-min liquid chromatography, where peptides were separated by polarity using a C-18 reverse phase column, and the following peptide fragmentation by the mass spectrometer Orbitrap Exploris 240 (Thermo Scientific). The analysis software used was Proteome Discoverer (Thermo Scientific). MS/MS data was sent to MASCOT and was used to search against a combination of the *P. chrysogenum* Uniprot database and the list of our rationally designed variants.

2.7. Antimicrobial activity assays

Fungal growth inhibition assays were conducted in 96-well microtiter plates (Nunc) in a total volume of 100 μL. Flat bottom plates were used for filamentous fungi assays and round bottom plates were used for yeast assays. 50 μL of 2× concentrated conidia (2.5×10^4 conidia/mL, final concentration) in 10 % potato dextrose broth (PDB) containing 0.02 % (*w/v*) chloramphenicol to avoid bacteria contamination were mixed in each well with 50 μL of 2× concentrated protein from serial twofold dilution (final concentrations range from 0.25 to 64 μg/mL depending on the fungus). Samples were prepared in triplicates. Plates were statically incubated for 72–96 h at 25 °C. Growth was determined every 24 h by measuring the optical density at 600 nm (OD600) using a plate spectrophotometer (SPECTROstar Nano, BMG Labtech) and the OD600 mean and standard deviation (SD) were calculated. Dose-response curves were generated from measurements after 72 h. The experiments were repeated at least twice. Minimum inhibitory concentration (MIC) is defined as the protein concentration that completely inhibited growth in all the experiments performed.

2.8. Protein-lipid overlay assays

To test the binding properties of AFPs, a protein-lipid overlay experiment was performed using PIP Strips that are spotted with 100 pmol of various biologically active lipids (Echelon Biosciences, Salt Lake City, UT). Strips were incubated with PBS/3 % fatty acid-free BSA for 120 min at RT to block non-specific binding. The lipid strips were then incubated with each AFP (1 μg/mL for PeAfpA, PeAfpB and PeAfpC; 5 μg/mL for chimeras) diluted in PBS/1 % fatty acid-free BSA for 60 min at 4 °C and washed thoroughly for 30 min (3 × 10 min) at 4 °C with PBS/0.1 % Tween-20. The next step was to incubate the strips with the specific rabbit polyclonal antibodies anti-PeAfpA, anti-PeAfpB or anti-PeAfpC, diluted 1:2500, 1:1000 and 1:2500, respectively [31]. Chimeras were detected with the anti-PeAfpB antibody (dilution 1:500). Incubation was performed overnight at 4 °C with gentle agitation. Then, lipid strips were washed thoroughly for 30 min (3 × 10 min) at 4 °C with PBS/0.1 % Tween-20 and incubated for 60 min at 4 °C with ECL NA934 horseradish peroxidase donkey anti-rabbit (Cytiva Life Sciences) diluted 1:20,000 with PBS/1 % fatty acid-free BSA. Finally, the strips were washed for 30 min (3 × 10 min) at 4 °C with PBS/0.1 % Tween-20 and chemiluminescent detection was performed with ECL-Select Western blotting detection reagent (Cytiva Life Sciences) using the Amersham Imager 680 (Cytiva Life Sciences). The experiments were repeated at least twice.

2.9. Protein crystallization and data collection

PeAfpB crystals (wild type and chimeric forms) grew in hanging drops at 21 °C using vapour-diffusion method. Initial crystallization trials were set up in the Cristalogenesis service of the IBV-CSIC using commercial screens JBS I, JBS II (JENA Biosciences) and JCSG (Molecular Dimensions) in 96-well plates (Swissci MRC2) using 0.3 μL of protein at 40 mg/mL in buffer A (25 mM Tris buffer pH 8, 200 mM NaCl) and 0.3 μL of mother liquor. PeAfpB crystals were obtained using 30 % Jeffamine M60C and 10 % DMSO as mother liquor. Crystals of chPeAFPV1 were obtained using 3.5 M ammonium sulphate, 1 % MPD and 0.1 M MES pH 6.5 as mother liquor. Crystals of chPeAFPV3 and chPeAFPV4 were obtained using 30 % PEG400, 0.1 M Hepes pH 7.5 and 0.2 M magnesium chloride as mother liquor. Crystals of chPeAFPV5 were obtained using 70 % MPD and 0.1 M Hepes as mother liquor. In all cases, crystals grew in 7–14 days and were directly flash frozen in liquid nitrogen from the screening plates. Crystals were tested in different beamlines of ALBA, ESRF (European Synchrotron Radiation Facility) and DLS (Diamond Light Source) synchrotrons. Diffraction data was collected at 100 K from single crystals at XALOC beamline of ALBA Synchrotron for PeAfpB, chPeAFPV1 and chPeAFPV5 and at ID23–2 beamline from ESRF Synchrotron for chPeAFPV3 and chPeAFPV4. Wavelength used was 0.87313 for chPeAFPV3 and chPeAFPV4, 0.97918 for PeAfpB and chPeAFPV1 and 0.97926 for chPeAFPV5. Data sets were processed using XDS [40] and reduced with Scala [41] (CCP4). The data-collection statistics for data sets used in structure determination are shown in Table S3.

2.10. Phase determination, model building and refinement

Crystal structures of PeAfpB and chimeras were solved by molecular replacement with MOLREP [42]. To solve PeAfpB structure, PAF coordinates (6HA4) were used as search model. The refined PeAfpB structure (PDB 7ZTF) was used to solve chPeAFPV1, chPeAFPV3, chPeAFPV4 and chPeAFPV5 structures. The final models for all the structures were completed by alternating several rounds of manual building with COOT [43] and automatic refinement with REFMAC [44]. Refinement statistics are summarized in Table S3. Figures for structural representations were generated with Pymol software (https://pymol.org/2; Schrödinger) including the APBS module for electrostatic potentials surface calculation [45].

3. Results

3.1. Crystal structure of PeAfpB

To get insights into the mechanisms of action of AFPs we tackle the PeAfpB structural characterization. PeAfpB generates high quality crystals that belong to space group $P3_221$ and diffract to 1 Å resolution (Table S3). Using as a model the structure of *P. chrysogenum* PAF (PDB 6HA4) we get phases by molecular replacement that allowed us to build the structure of one PeAfpB molecule in the crystal asymmetric unit at atomic resolution (Fig. 1). The PeAfpB protomer presents the characteristic Greek key fold previously observed in other AFPs [5], showing five antiparallel β-strands (β1 from Lys3 to Ser9, β2 from Thr14 to Lys19, β3 from Lys22 to Lys27, β4 from His41 to Asp46 and β5 from Thr51 to Asp53) organized in two β-sheets, A and B, which are disposed orthogonally building a β-barrel (Fig. 1A and B). β-sheet A comprises β1, β4 and β5 while β-sheet B comprises β1, β2 and β3 strands participating the long and twisted β1-strand in both β-sheets (N- and C-terminal portion in β-sheets A and B, respectively). The twisted conformation of β1 is allowed by the presence of two consecutive Gly residues (Gly5 and Gly6) followed by a Cys (Cys8), which is disulfide-bonded to Cys36, pulling the strand towards the center of the protein. Loops connecting β1-β2 (L1), β2-β3 (L2) and β4-β5 (L4) strands are short (2–4 residues) while loop connecting β3-β4 (L3) strands is long (14 residues) and divided in two portions by the presence of Cys36 that anchors the loop to the protein main-body by a disulfide bond with Cys8 in β1. In total, PeAfpB has six Cys residues (Cys8, Cys15, Cys28, Cys36, Cys43 and Cys54), that form three intramolecular disulfide bridges connecting Cys8-Cys36, Cys15-Cys43 and Cys28-Cys54 residues (Fig. 1A and B).

Structural comparison of PeAfpB with the AFPs available in the PDB showed an extraordinary structural conservation within class A and B members. Main-chain superposition of the complete molecules (notice that some structures have been solved by nuclear magnetic resonance [NMR] spectroscopy) gives root-mean-square deviations (RMSDs) values between 1.0 and 1.9 Å (Fig. 1C). This structural conservation is not surprising for the phylogenetically related class B member PAFB from *P. chrysogenum*, with which PeAfpB presents a sequence identity of 77 % (RMSD <1.0 Å for the superimposition of 57 residues). However, it is more striking for the phylogenetically distant class A member PAF from *P. chrysogenum,* with which PeAfpB only has a 48 % identity, but also shows an RMSD of 1 Å (superimposition of 54 residues) (Fig. 1B and C). Similarly, low RMSDs (1.3 and 1.7 Å) were calculated for the superimposition with class A *A. giganteus* AFP and NFAP structures, with which sequence identity is lower than 45 %, confirming the extremely conserved fold of both AFP classes. Notice that this structural similarity is not restricted to the β-strands, but also the loops show identical

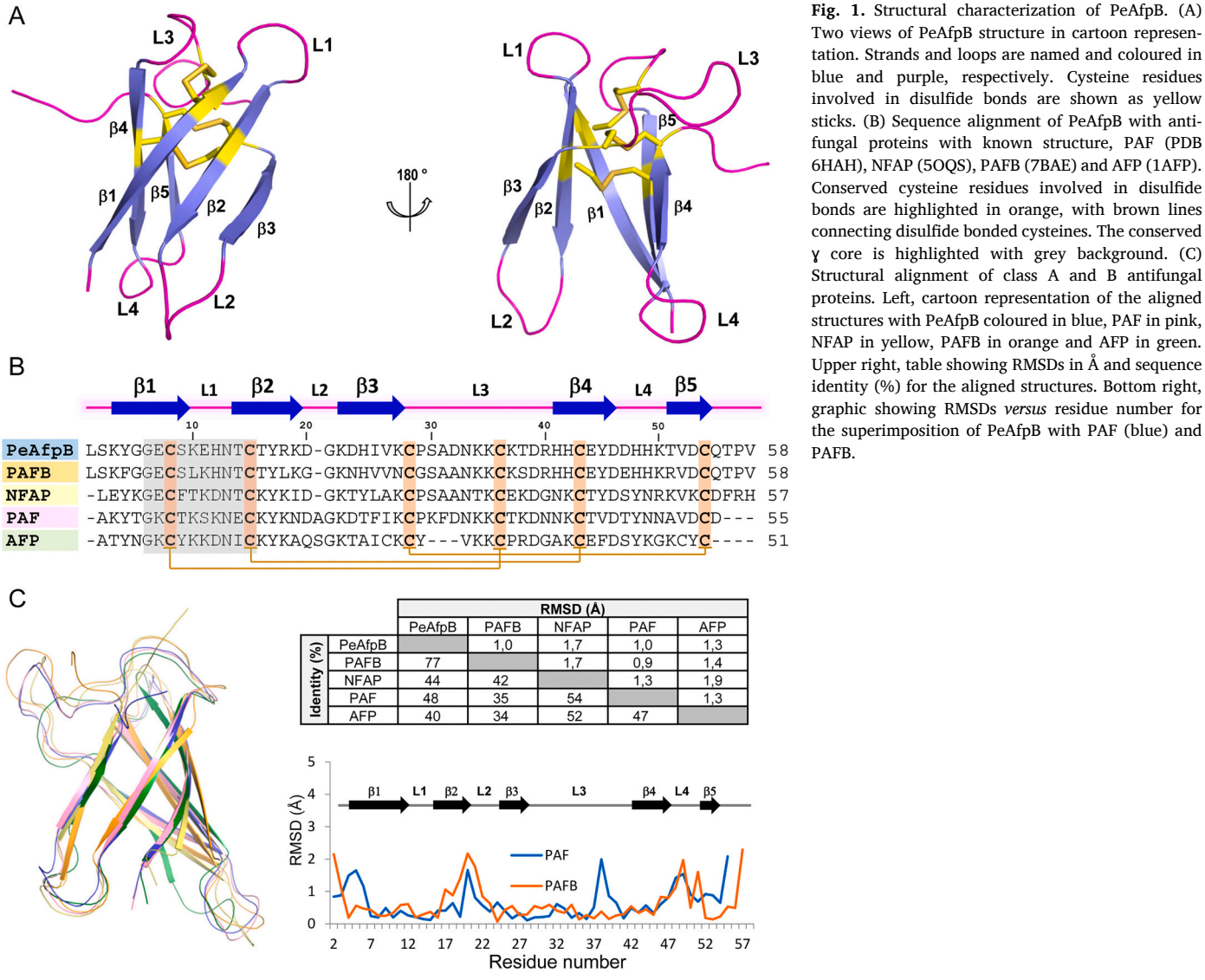

Fig. 1. Structural characterization of PeAfpB. (A) Two views of PeAfpB structure in cartoon representation. Strands and loops are named and coloured in blue and purple, respectively. Cysteine residues involved in disulfide bonds are shown as yellow sticks. (B) Sequence alignment of PeAfpB with antifungal proteins with known structure, PAF (PDB 6HAH), NFAP (5OQS), PAFB (7BAE) and AFP (1AFP). Conserved cysteine residues involved in disulfide bonds are highlighted in orange, with brown lines connecting disulfide bonded cysteines. The conserved γ core is highlighted with grey background. (C) Structural alignment of class A and B antifungal proteins. Left, cartoon representation of the aligned structures with PeAfpB coloured in blue, PAF in pink, NFAP in yellow, PAFB in orange and AFP in green. Upper right, table showing RMSDs in Å and sequence identity (%) for the aligned structures. Bottom right, graphic showing RMSDs *versus* residue number for the superimposition of PeAfpB with PAF (blue) and PAFB.

conformational disposition in all the analyzed structures, even in the long L3 loop connecting β3 and β4 strands (Fig. 1C).

On the contrary, the structural comparison with the class C AFPs (BP protein from *Penicillium brevicompactum* and *P. chrysogenum* PAFC) showed only a very limited structural similarity reduced to the three strand PeAfpB β-sheet A (Fig. S2), confirming the phylogenetic distance of class C AFPs with classes A and B.

3.2. Rational design of PeAfpB::PeAfpA chimeric proteins

Our previous studies showed that PeAfpA presents higher antifungal activity than PeAfpB against plant and animal pathogens [31]. Given that PeAfpA and PeAfpB share only 40 % sequence identity (Fig. 2A), we hypothesized that areas of higher sequence variability may be implicated in this differential antifungal activity. Our PeAfpB based structural analysis shows the exquisite folding conservation for AFPs of A and B classes, including the loops connecting the β-strands (Fig. 1C). This observation implies that class A and B AFPs share a highly conserved and stable structural scaffold which would allow sequence variations with implications in antifungal activity and specificity. To test this possibility and to get insight into structure-activity relationship of AFPs we design PeAfpB::PeAfpA chimeric proteins guided by the PeAfpB 3D structure. To design chimeric PeAfpB::PeAfpA proteins, residues in loops L1, L2, L3 and L4 as well as the C-terminus of PeAfpB were substituted by those of PeAfpA (Fig. 2A and B) to generate chPeAFPV1-V5. Notice that these areas not only exhibit greater sequence variability between PeAfpA and PeAfpB than the rest of the protein motifs but they are also the areas with high sequence variability within each class of AFPs (Fig. 1B and Fig. 2A). In chPeAFPV1, the PeAfpB Glu11 and His12 residues located in loop L1 within the conserved γ-core motif were substituted for the PeAfpA Lys10 and Asp11 residues, which corresponds to a reverse charge exchange in this region at physiological pH. The chimera chPeAFPV2 resulted from a seven residues substitution spanning from the last residues of β2 to the beginning of β3 strands and including the interposed loop L2, while chPeAFPV3 arises from substitution of six residues between Cys36 and Cys43 corresponding to the second part of the long loop L3 and the initial part of β4 strand. In chPeAFPV4, five residues spanning the loop L4 and the first residue of β5 strand were interchanged with those of PeAfpA. Finally, chPeAFPV5 was obtained by swapping the four C-terminal residues (Fig. 2). Table 1 shows the predicted physicochemical properties of parental and chimeric proteins. With the exception of chPeAFPV3, for which the pI value was practically identical to that of PeAfpB (7.77 *vs* 7.80), all of the chimeras showed a pI value very similar (8.26–8.27) and slightly higher to that of PeAfpB (7.8) but none of them reached the PeAfpA pI value (9.48).

3.3. Recombinant production and purification of chPeAFPs

To evaluate the structural and functional role of the substitutions introduced in the different chimeras, we used the *P. chrysogenum*-based expression cassette [11], adapted to the FB platform [34] for protein recombinant production. The five rationally designed chPeAFPs were produced in *P. chrysogenum* under the regulation of the strong *paf* promoter and terminator sequences, using their corresponding native signal peptide (SP)-pro sequences (Fig. 3A). In addition, the PeAfpB production in *P. chrysogenum* was addressed as an internal control.

Several *P. chrysogenum* positive independent transformants were obtained (Fig. S1), and after evaluation for protein production, one clone for each construction with the highest production of PeAfpB and chPeAFPs was selected for further characterization. The selected recombinant strains were PCGL19032, PCGL19213, PCGL19451, PCGL19661, PCGL19812 and PCGL20031 for PeAfpB and chPeAFPV1-

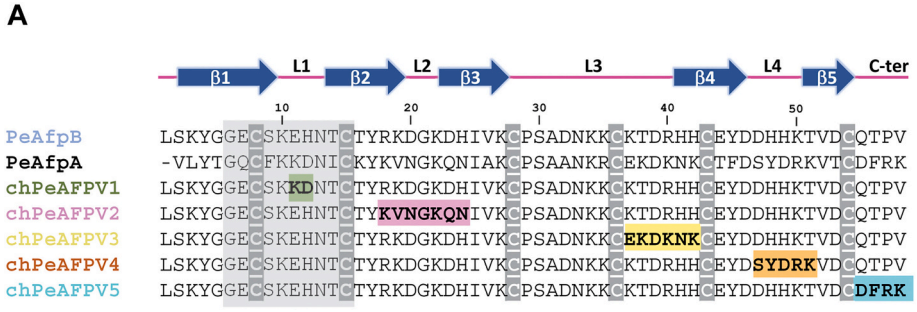

Fig. 2. Design of PeAFP chimeras. (A) Sequence alignment of PeAfpB, PeAfpA and the designed chimeras. Amino acids exchanged between PeAfpB and PeAfpA to generate the chimeras are highlighted in green for chPeAFPV1, pink for chPeAFPV2, yellow for chPeAFPV3, orange for chPeAFPV4 and cyan for chPeAFPV5. The conserved ɣ core is represented as a grey box. At the top of the alignment is shown the PeAfpB secondary structure with arrows and lines for β-sheets and coiled regions, respectively. Cysteine residues are underlined and highlighted in grey. (B) Cartoon representation of PeAfpB structure using the same colour code as in (A) to visualize the location of the substitutions.

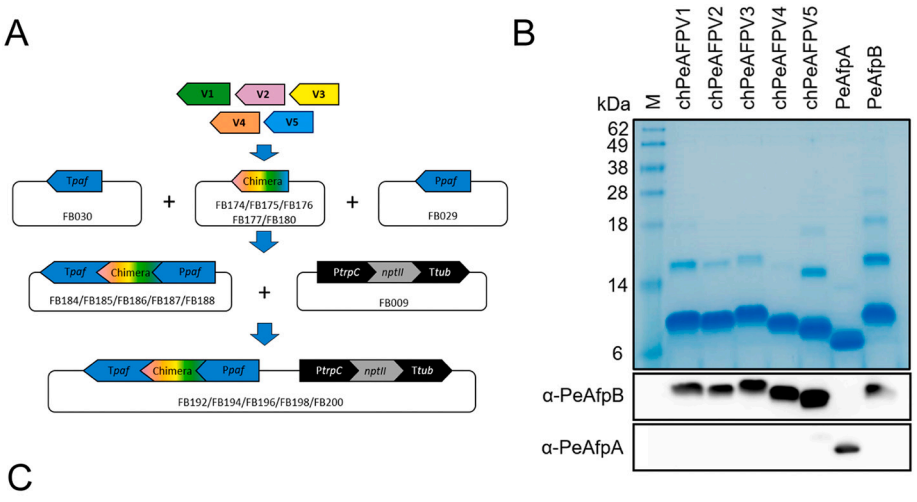

Fig. 3. Production, purification and identification of parental and chimeric PeAFPs. (A) Schematic diagram of the modular assembly of each chimera genetic sequence into pUPD2 vectors with FB030 and FB029 (*paf* promoter and terminator sequences, respectively) to obtain pDGBα1R plasmids FB184, FB185, FB186, FB187 and FB188 and a subsequent binary assembly of these plasmids with FB009 to obtain final pDGBΩ1 vectors FB192, FB194, FB196, FB198 and FB200 for *P. chrysogenum* transformation. (B) SDS-PAGE gel of the five purified chPeAFPs (2 μg per sample). Two μg of pure PeAfpA and PeAfpB were also added as controls. Immunodetection with α-PeAfpA and α-PeAfpB is also shown. (C) Peptide mass fingerprinting (PMF) of PeAfpB and chimeras. In brackets, percentage (%) of primary sequence covered by PMF. Amino acids exchanged are highlighted in green (chPeAFPV1), pink (chPeAFPV2), yellow (chPeAFPV3), orange (chPeAFPV4) and cyan (chPeAFPV5).

C

```
PeAfpB:     LSKYGGECSKEHNTCTYRKDGKDHIVKCPSADNKKCKTDRHHCEYDDHHKTVDCQTPV
(69%)       LSKYGGECSKEHNTCTYR
                           KDGKDHIVKCPSADNK
                               DHIVKCPSADNKKCK
                                   CPSADNKKCKTDR
chPeAFPV1:  LSKYGGECSKKDNTCTYRKDGKDHIVKCPSADNKKCKTDRHHCEYDDHHKTVDCQTPV
(69%)       LSKYGGECSKKDNTCTYR
                           KDGKDHIVKCPSADNKK
                               DHIVKCPSADNKKCK
                                   CPSADNKKCKTDR
chPeAFPV2:  LSKYGGECSKEHNTCTYKVNGKQNIVKCPSADNKKCKTDRHHCEYDDHHKTVDCQTPV
(100%)      LSKYGGECSKEHNTCTYKVNGK
               YGGECSKEHNTCTYKVNGKQNIVK
                     EHNTCTYKVNGKQNIVKCPSADNKK
                         VNGKQNIVKCPSADNKKCK
                             QNIVKCPSADNKKCKTDR
                                   CPSADNKKCKTDR
                                               HHCEYDDHHKTVDCQTPV
chPeAFPV3:  LSKYGGECSKEHNTCTYRKDGKDHIVKCPSADNKKCEKDKNKCEYDDHHKTVDCQTPV
(100%)      LSKYGGECSKEHNTCTYR
               YGGECSKEHNTCTYR
                           DGKDHIVKCPSADNKKCEK
                                   CPSADNKKCEKDKNK
                                       KCEKDKNK
                                         DKNKCEYDDHHK
                                             CEYDDHHKTVDCQTPV
chPeAFPV4:  LSKYGGECSKEHNTCTYRKDGKDHIVKCPSADNKKCKTDRHHCEYDSYDRKVDCQTPV
(79%)       LSKYGGECSKEHNTCTYR
                           KDGKDHIVKCPSADNKK
                            DGKDHIVKCPSADNKKCK
                                               HCEYDSYDR
chPeAFPV5:  LSKYGGECSKEHNTCTYRKDGKDHIVKCPSADNKKCKTDRHHCEYDDHHKTVDCDFRK
(83%)       LSKYGGECSKEHNTCTYR
                           KDGKDHIVKCPSADNKK
                               DHIVKCPSADNKKCKTDR
                                                     TVDCDFRK
```

V5, respectively. The growth of the selected strains in solid medium, PDA and PcMM, was indistinguishable from those of the reference strain *P. chrysogenum* Q176 and the parental *P. chrysogenum* strain Δ*paf* used for transformation (Fig. S1).

Selected strains for protein production were grown in liquid PcMM, and after clearing the culture broth from insoluble matter, the proteins in the supernatants were purified by one-step cation-exchange chromatography. Optimal production was achieved after 5 days of growth, with yields of 120 mg/L, 32 mg/L, 29 mg/L, 18 mg/L, 15 mg/L and 145 mg/L for PeAfpB and chPeAFPV1-V5 respectively. All of them eluted as single peaks in a range of saline gradient from 0.1 to 0.23 M in accordance with their theoretical pI values. SDS-PAGE analysis (Fig. 3B) revealed faint protein bands of apparent molecular masses higher than 6 kDa, whose percentage between chimeras were negligible, corresponding to possible oligomers. As described for other AFPs, anomalous migration was observed in some of the chimeras; chPeAFPV5 (6.81 kDa) showed faster migration than expected compared to the slightly smaller PeAfpB (6.69 kDa). This behavior seems to be related to the extreme isoelectric point of these proteins. In addition, western blot analyses of purified chimeric proteins were performed with antibodies raised against PeAfpB and PeAfpA [31]. Results indicated that all chimeric proteins reacted with anti-PeAfpB antibody (Fig. 3B). By contrast, only purified chPeAFPV5 showed a very faint immunoreaction with anti-PeAfpA antibody.

Finally, the identity of the variants was successfully verified by peptide mass fingerprinting (LC-ESI-MS/MS) of the derivatised and trypsin-digested in-gel bands. As can be seen in Fig. 3C, sequence coverage of primary sequences ranging from 69 % to 100 % was reached. Peptides covered 69 % of PeAfpB and chPeAFPV1, 79 % of chPeAFPV4, 83 % of chPeAFPV5 and 100 % of chPeAFPV2 and chPeAFPV3 primary sequences. Note that all amino acid substitutions introduced were identified in the corresponding variant. Moreover,

proper protein processing in the N-terminal region, in which the SP-pro peptide is cleaved out, was observed.

3.4. chPeAFPs show significant differences in their antifungal activity

The antifungal activity of the five chPeAFPs was tested and compared to that of parental PeAfpB and PeAfpA against a selection of filamentous fungi. This selection includes plant pathogens such as the citrus fruit specific *P. digitatum*, the polyphagous *B. cinerea,* the blue mould *P. expansum,* the rice blast fungus *M. oryzae* and the soilborne plant pathogen *F. oxysporum.* Furthermore, the fruit juice contaminant *B. spectabilis,* which is particularly sensitive to AFPs [32] was also examined. Finally, to evaluate the anti-yeast activity, *S. cerevisiae* was also tested.

Differences in antifungal activity were observed among the AFPs tested. Table 2 shows MIC values of parental and chimeric proteins against all fungal species evaluated. In accordance with previous results, PeAfpA inhibited the growth of all tested species while PeAfpB showed a moderate activity against some of the filamentous fungi and, at the highest concentration tested (64 μg/mL), it was not active towards *F. oxysporum*, *M. oryzae* and *S. cerevisiae* (Table 2) [31,32]. Regarding chPeAFPs, chPeAFPV1 and chPeAFPV2 improved the parental PeAfpB antifungal activity with MIC values very similar to those showed by PeAfpA against *B. cinerea*, *B. spectabilis*, *P. expansum* and *P. digitatum*. Notably, the change of only two residues (Glu11 and His12 for Lys10 and Asp11) in chPeAFPV1 promotes identical activity than PeAfpA for these organisms, and seems to improve it against *P. expansum*. However, both variants behaved similar to PeAfpB against *F. oxysporum, M. oryzae* and *S. cerevisisae,* since they were inactive at the highest concentration tested. Of note was the lack of activity of chPeAFPV3 towards most of the fungi tested, with the exception of *B. spectabilis*, which resulted to be the most sensitive fungus to all the tested proteins. The lack of antifungal activity of chPeAFPV3 points out the significance of residues 37–42 in the antifungal activity of PeAfpB. Finally, chPeAFPV4 and chPeAFPV5 showed an intermediate profile of antifungal activity compared to the parental proteins.

3.5. Structural characterization of chPeAFPs

To understand the molecular basis of the variation in antifungal activity exhibited by chPeAFPs, we undertook their structural characterization. We obtained crystals for all the variants except for chPeAFPV2, which did not crystallize in any of the different screening alternatives used for the crystallization of the other chimeras. Crystals from variants chPeAFPV1, chPeAFPV3, chPeAFPV4 and chPeAFPV5 diffract to atomic resolution (1.0–1.3 Å) as parental PeAfpB. Surprisingly for crystals obtained under completely different crystallization conditions, from ammonium sulfate to PEGs or MPD (see Materials and Methods), all of them showed identical space group and unit cell to the parental PeAfpB (Table S3), indicating the same protein packing regardless of the crystallized chimera. This observation would suggest that the proteins should present a very similar conformation with preferential way to be organized into the crystal. The analysis of the structures confirms this point, showing all the chimeras an almost identical conformation to PeAfpB structure (Fig. 4 and Fig. S3), although changes in the electrostatic potential surfaces are observed among the chimeras (Fig. S4). The conserved crystallization cell and space group explains why we were unable to crystallize chPeAFPV2, since the exchanged region in this chimera makes multiple contacts, including salt bridges, with other three symmetric molecules in the crystal, playing a key role in the packing (Fig. S5). The superposition of all (parental and chimeras) structures yielded extremely low global RMSDs, between 0.19 and 0.41 Å, with the exception of chPeAFPV5 which showed deviations over 1 Å (Fig. 4B). Interestingly, although chPeAFPV5 changes are small, they localize not only at the C-terminal end, which was the interchanged portion, but also in loops L3 and L4. The differences in these regions are not due to conformational changes in the skeleton but to contacts between the new C-terminal side-chains and the residues in loops L3 and L4 (Fig. 4). It is striking the minimal conformational changes induced by the swapping, some of them involving >10 % of the molecule. A detailed look at the exchanged areas shows that the main-chain of the different chPeAFPs is not altered, presenting only the new side chains as different (Fig. 4A). Therefore, the differences in the antifungal activity observed among chPeAFPs are purely due to the contributions of specific residues and not to induced conformational changes or structural rearrangements. This is notable in chPeAFPV3, which is basically inactive, but whose structure shows minimal conformational change with respect to parental PeAfpB (RMSD 0.34 Å). These results, together with the initial structural analysis of class A and B AFPs, also confirms the structural optimization defined by the scaffold of these proteins.

3.6. Protein O-mannosylation is important for interaction of PeAFPs and chPeAFPs with the cell wall

To examine the role of the cell wall in the mode of action of parental AFPs and chimeras, we characterized the response to all of them of the *Pdpmt2* deletion mutant strain. This strain is a *P. digitatum* null mutant on the O-mannosyltransferase 2 (Δ*pmt2*) that affects protein mannosylation, including the mannoproteins on the outer cell wall. *Pdpmt2* is known to have cell wall defects and greater tolerance to antifungal peptides and proteins such as PAF26 [37] and PdAfpB [15].

Growth inhibition assays showed that the Δ*pmt2* mutant was much more tolerant to both native and chimeric proteins than the wild-type strain (Table 2 and Fig. 5). In the conditions tested, only PeAfpA completely inhibited the growth of the mutant; however, the MIC value (32 μg/mL) was significantly higher than that showed against *P. digitatum* wt strain (1 μg/mL). Chimeras chPeAFPV1 and chPeAFPV2, with similar MIC values to that of PeAfpA against *P. digitatum* wt strain, did not reach MIC values against Δ*pmt2*, although approximately a 50 % growth reduction was observed at the highest concentration tested. Finally, PeAfpB and the chimeras chPeAFPV3, chPeAFPV4 and chPeAFPV5 were inactive against Δ*pmt2*. Altogether, these results suggest that mannoproteins determine protein interaction with the cell wall and, thus, its antifungal activity.

3.7. Antifungal activity and phospholipid recognition

To gain further insights into the role of fungal plasma membrane in the killing mechanism of PeAFPs and chimeras, their potential interaction with biologically relevant phospholipids was evaluated. To assess

Table 2
Minimum inhibitory concentration (MIC) (μg/mL) of parental and chimeric antifungal proteins.

Microorganism	PeAfpA	PeAfpB	chPeAFPV1	chPeAFPV2	chPeAFPV3	chPeAFPV4	chPeAFPV5
B. spectabilis	1	8	1	2	16	4	4
B. cinerea	4	32	4	8	>64	32	32
F. oxysporum	4	>64	>64	>64	>64	>64	>64
M. oryzae	16	>64	>64	>64	>64	>64	>64
P. expansum	4	32	2	4	>64	64	16
P. digitatum	1	8	1	2	>64	4	4
S. cerevisiae	8	>64	>64	>64	>64	>64	>64

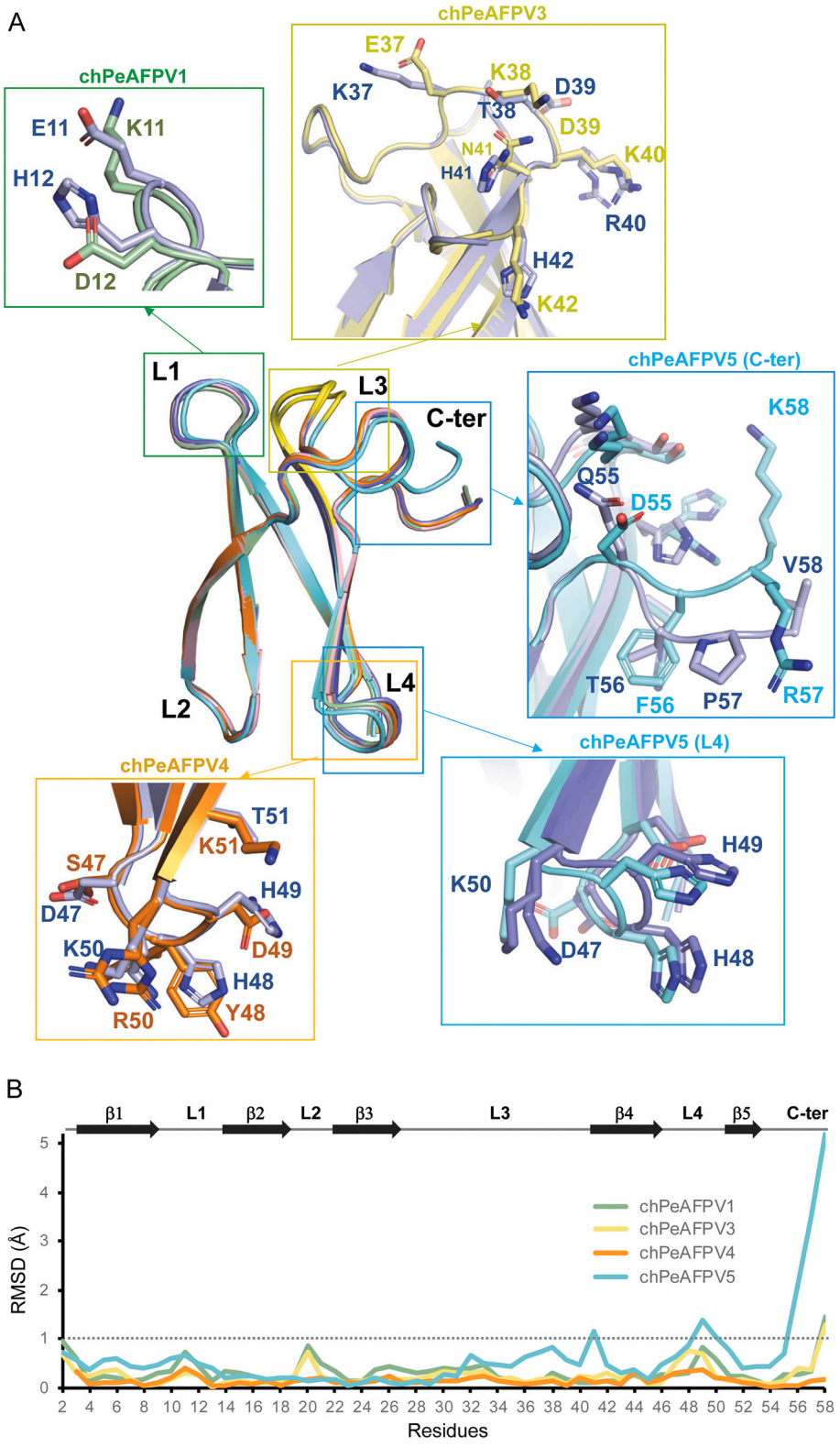

Fig. 4. Structural characterization of PeAFP chimeras. (A) Superposition in cartoon representation of PeAfpB (blue), chPeAFPV1 (green), chPeAFPV3 (yellow), chPeAFPV4 (orange) and chPeAFPV5 (cyan) structures. A close view of the interchanged areas in each chimera is depicted showing the superimposed structures of PeAfpB with the corresponding chimera and with the swapped residues in sticks and labeled. For chPeAFPV5, in addition to the interchanged area, a close view of loop L4 region is also shown, as it shows a slight movement. (B) Graphic showing RMSDs *versus* residue number for the superimposition of PeAfpB with the PeAFP chimeras using the same colour code as in (A). The conserved secondary structure for the structures is schematized at the top of the graphic.

the ability of proteins to bind to membrane phospholipids we performed a protein-lipid overlay assay using a commercial lipid strip with fifteen immobilized phospholipids on the surface. Fig. 6A shows the lipid binding profile of native proteins PeAfpA and PeAfpB. The class C AFP from *P. expansum*, PeAfpC, was also included since this protein is the least active of the three PeAFPs against a wide number of pathogenic fungi, although it shows a powerful inhibition against the food spoilage fungus *B. spectabilis* [31,32]. We found that PeAfpA and PeAfpB bind to all phosphoinositides but not to the dephosphorylated compound phosphatidylinositol (PtdIns). Quantification of the relative binding to lipid strips was achieved by performing densitometry analysis on two independent experiments (Fig. S6). Both proteins strongly bind to phosphatidylinositol monophosphates (PtdIns(3)P, PtdIns(4)P and PtdIns(5)P) while a moderate binding to phosphatidylinositol

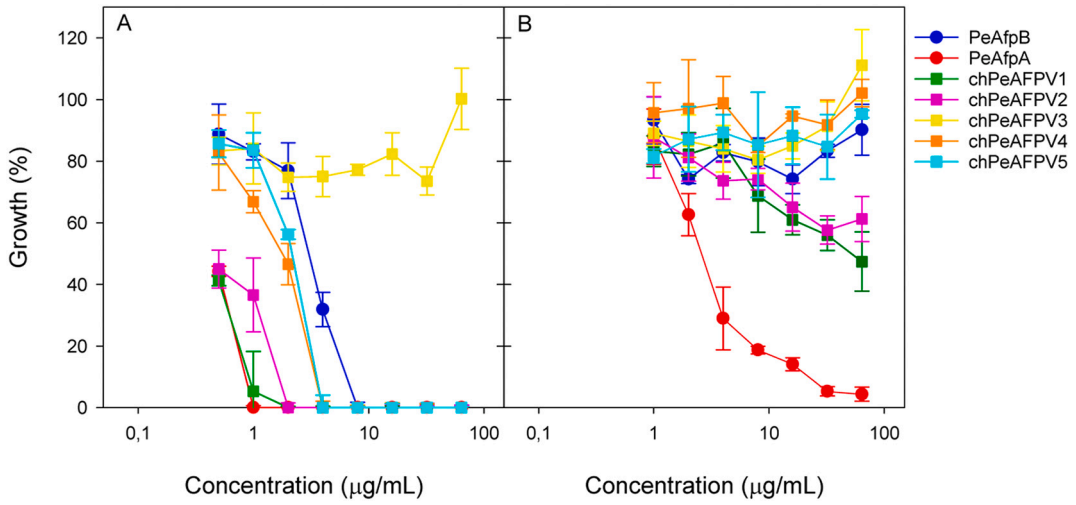

Fig. 5. *In vitro* inhibitory activity of parental and chimeric PeAFPs. Dose-response curves against *P. digitatum* wt (A) and Δ*pmt2* mutant strain (B). Curves show the means ± SD from triplicate values at an optical density of 600 nm (OD600) after 72 h of incubation.

bisphosphates (PtdIns(3,4)P_2, PtdIns(3,5)P_2 and PtdIns(4,5)P_2) and a faint binding to phosphatidylinositol triphosphate (PtdIns(3,4,5)P_3) was observed. Both PeAFPs also show a moderate binding to phosphatidic acid (PA) and a weaker binding to phosphatidyletanolamine, phosphatiylserine and lysophosphatidic acid. None of them bind to lysophosphatidylcoline, phosphatidylcoline or sphingosine 1-phosphate. Notably, a lack of binding to any of the lipids tested was found for PeAfpC.

Next, we examined the interaction of chimeras with membrane phospholipids (Fig. 6B). Three of them, chPeAFPV1, chPeAFPV4 and chPeAFPV5, showed a binding capability similar to that of the parental proteins PeAfpA and PeAfpB. Interestingly, the inactive variant chPeAFPV3 behaved like PeAfpC, and no lipid binding was observed. This observation seems to support a correlation between phospholipid binding and antifungal activity as in the case of PeAfpC. However, the highly active variant chPeAFPV2, whose antifungal activity is similar to that of PeAfpA and chPeAFPV1 (Table 2), behaved like PeAfpC and chPeAFPV3 and no lipid binding capability was observed. Residues substitution for chPeAFPV2 and chPeAFPV3 are located on opposite sides of the molecule (Fig. 2), so the lack of binding is not due to modification of a specific lipid site, suggesting that lipid recognition and binding is complex and/or polyvalent. In addition, the results of chPeAFPV2 indicate that the antifungal activity of AFPs does not always need previous binding to lipid membranes. However, we cannot rule out that binding to other phospholipids not tested here may also contribute to the antifungal activity. Structural characterization of AFPs in complex with phospholipids would shed light on this point.

4. Discussion

In this study, we provide detailed insight into the 3D structure by X-ray crystallography of PeAfpB from the phytopathogenic fungus *P. expansum*, and of four PeAfpA::PeAfpB chimeras, whose antimicrobial activity and potential molecular targets are also described. PeAfpB is one of the three AFPs encoded in the genome of *P. expansum*, it shows moderate antifungal activity and belongs to the B phylogenetic class within the AFP family [31]. By contrast, the 3D structures of the other two *P. expansum* proteins, PeAfpA and PeAfpC, are unknown and their structural characterization as well as that of one of our chimeras, chPeAFPV2, remain elusive.

So far, only one member of class B AFPs, *P. chrysogenum* PAFB, has been structurally characterized. The 3D structure of an N-terminal short form of PAFB (sfPAFB; 56 instead of 58 amino acids) was initially solved by NMR spectroscopy [13], and later the X-ray crystal structure of the mature full-length PAFB was solved [46] showing identical fold and small conformational differences due to the different techniques used. Regarding class A, the structures of the deeply characterized AFP from *A. giganteus* and PAF from *P. chrysogenum* were solved by NMR spectroscopy [5,47], as well as that of *N. fischeri* NFAP [48]. Similar to that observed here for PeAfpA, PAF was described as recalcitrant to crystallization, and only co-crystallization with calixarene led to the production of crystals to solve the structure at high-resolution [49]. Instead, the structure of the class C BP protein from *P. brevicompactum* was solved by X-ray crystallography [50], and recently, the structure of PAFC was determined by NMR spectroscopy [51]. Our analysis of these available structures shows an exquisite conservation in the folding for the AFPs of classes A and B, not only in the secondary structure elements conforming the core β-barrel, but also in the loops that connect them and that usually present a greater conformational freedom. Although a similar folding might be expected, differences greater than the observed (RMSD <1 Å) should be expected for proteins with sequence identities <40 % [52], indicating that the structural scaffold of these AFPs has been highly optimized to allow sequence variations. In contrast, the folding of AFPs from class C shows a lower structural homology, with only partial conservation of one of the β-sheets that form the structural core of these proteins, pointing to a much greater phylogenetic distance or an independent origin.

The preservation of the structural scaffold for class A and B AFPs opens the door to the realization of protein engineering studies for structure-function knowledge generation and/or biotechnological purposes, as well as for the very precise *in silico* characterization, using software such as AlphaFold [53], of the folding of those antifungal proteins with unknown structure. We prove this point by designing five chPeAFPs, in which high variable residues from loops connecting the core β-strands and the C-terminal end of PeAfpB sequence were substituted by those corresponding to PeAfpA. All chPeAFPs were produced using the *P. chrysogenum*-based expression cassette [11], confirming the tolerance of the AFP core for modification and the suitability of the expression system for producing AFP chimeras [11–13,25,26,31,54,55]. Here, all the swaps were tolerated and the proteins were expressed and purified in high yields (from 15 to 145 mg/L) confirming that these changes do not impair protein production and secretion. Remarkably, the four chimeric proteins whose 3D structure was obtained showed almost identical fold, validating the high stability of the AFP scaffold. Interestingly, the chimeras showed a wide range of antifungal activity and interaction with specific cell wall and membrane components, from those more similar to PeAfpA to almost total loss of these capacities. We therefore conclude that the observed differences are

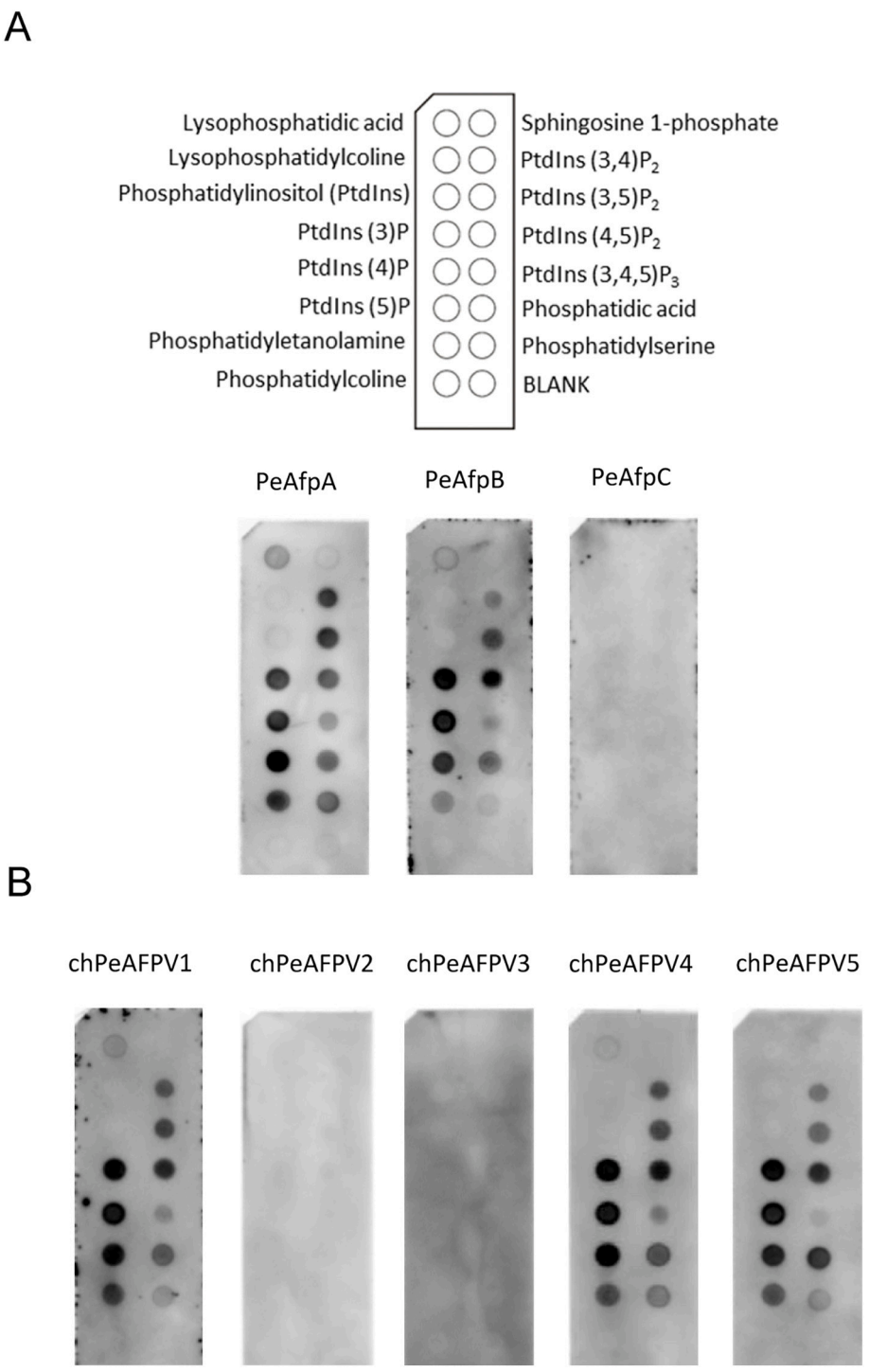

Fig. 6. Lipid binding profile of parental and chimeric PeAFPs. Ability of parental (A) and chimeric PeAFPs (B) to bind phospholipids in protein-lipid overlay assays.

directly related to the amino acid residues exchanged. Moreover, our work confirms and extends previously reported data on how minor amino acid changes affect the properties of antifungal peptides and proteins [11,25,27,56,57].

The antifungal activity showed by each of the chimeras revealed the relevance of the substitutions introduced in loops L1, L2 and L3. Replacement of only two residues (Glu11 and His12) in PeAfpB sequence by the corresponding from PeAfpA in loop L1 (Lys10 and Asp11), increased the antifungal activity of the chPeAFPV1 chimera to that of PeAfpA against *B. cinerea*, *B. spectabilis*, *P. expansum* and *P. digitatum*, but not against *F. oxysporum, M. oryzae* and *S. cerevisiae* (Table 2), suggesting a spatial distribution for species specificity antifungal elements in AFPs. These residues, located in loop L1, are within the conserved γ-core motif present in antimicrobial cysteine-rich proteins from prokaryotes and eukaryotes [6]. This motif was already found to be an important functional determinant of some antifungal plant defensins, although not every defensin γ-core exerts antifungal activity [58]. Similar results have been described for AFPs. For instance, the γ-core motif derived from NFAP2 and PdAfpB did not exhibit activity [28,55]. By contrast, a synthetic 14 amino acid long peptide fragment spanning the PAF γ-core motif displayed *in vitro* antifungal activity against *C. albicans*, and the correlation between the positive net charge

and hydrophilicity of the γ-core derivative peptide and the antimicrobial activity was demonstrated [26]. Moreover, the same amino acid exchanges in the γ-core motif of the full-length protein PAF comparably enhanced the antifungal efficacy of the respective PAF variants [26]. Here, two amino acid exchanges in the γ-core motif of the full-length protein PeAfpB enhanced the antifungal activity. The γ-core of PeAfpB (residues 6–15, Fig. 2A) is negatively charged at pH 7 (predicted net charge −0.9; http://protcalc.sourceforge.net) while in the chPeAFPV1 chimera it is nearly neutral (predicted net charge −0.1 at pH 7), and that of PeAfpA is slightly positively charged (predicted net charge 0.8 at pH 7). The γ-core of PAFB is also nearly neutral (residues 6–15, predicted net charge +0.1; Fig. 1B) and it did not exhibit antifungal activity, although the exchange of distinct amino acids to positively charged and hydrophilic ones rendered an active peptide [59]. Interestingly, when the optimized γ-core of PAFB was introduced in the full-length protein, the recombinant PAFB was readily degraded when homologously expressed, suggesting the role of the γ-core in PAFB structure and stability [59]. In this work, we have not characterized peptides spanning the γ-core motif; instead, we have designed full-length chimeras. Considering the full-length proteins, chPeAFPV1 is positively charged (+2.9) but much less than PeAfpA (+8.7) (Table 1), suggesting a lack of correlation between positive net charge and antifungal activity as described for PAF [26]. Furthermore, and considering that chPeAFPV1 is produced and correctly processed, the changes introduced in loop L1 do not affect protein stability, contrary to that described for PAFB [59].

Unexpectedly, substitution of six residues in the loop L3 of PeAfpB with those of PeAfpA (Fig. 2) rendered the chimera chPeAFPV3 inactive. The activity of isolated peptides spanning the loop L3 from two different proteins (PdAfpB and PAF) allowed establishing its relevance to antifungal activity [28]. Moreover, mutations of Lys35 and Lys38 [5] and of Phe31 [11], which are located in this loop L3 of PAF, negatively affect antifungal activity. Therefore, it was suggested that loop L3 is an important domain in the antifungal activity of AFPs, although additional protein motifs might also contribute to the antifungal activity. In addition, co-crystallization studies of PAF with anionic calixarenes revealed binding to loop L3 and thus it was hypothesized that this region of the protein might be involved in binding to negatively charge membrane phospholipids. Together with the role of loop L3 in antifungal activity [5,11], authors suggested that this region might be required for membrane binding which is a prerequisite for PAF antifungal activity [49]. Loop L3 of PAFB is also involved in calixarene binding, although a different binding site, through Lys residues, was identified at loop L2 [46]. In our work, substitutions to render chimera chPeAFPV3 were introduced in the second half of loop L3. This swapping decreased full-length protein charge from 2.2 to 1.7 (Table 1) and affected Lys37, a conserved amino acid in the active class B proteins PdAfpB and PAFB, suggesting the relevance in antifungal activity. By contrast, introduction of Lys38, Lys40 and Lys42 in the sequence did not favor antifungal activity, suggesting that not only the presence but also the position of Lys residues within the sequence is determinant for the antifungal activity. Interestingly, chPeAFPV3 chimera did not bind to the membrane phospholipids evaluated here, suggesting the relevance of loop L3, as described for PAF [49], in phospholipid binding. Also of note is the active chimera chPeAFPV2, whose substitutions in loop L2 enhanced antifungal activity towards some of the fungi evaluated, but impaired the binding to membrane phospholipids under the conditions tested. These results suggest that, as described for PAFB [46], loop L2 might be involved in membrane binding, but also that this binding does not seem to be a fundamental requisite for the antifungal activity of chPeAFPV2. Accordingly, some hybrids of defensins NaD1 and NaD2 were efficient antifungal molecules, even though they bound poorly to phospholipids [60].

From the three PeAFPs, the class C PeAfpC is the only one that does not bind to any of the membrane phospholipids tested. When firstly characterized, PeAfpC was described as inactive towards a selection of plant and human fungal pathogens [31]. However, recently PeAfpC was reported to show great effectiveness against *Byssochlamys* species, in particular against *B. spectabilis* strains [32]. Therefore, we can hypothesize that PeAfpC killing mechanism, like that of chPeAFPV2 and chPeAFPV3, does not require phospholipid binding. We could also speculate that *Byssochlamys* species present significant differences in the lipid composition of their cell membranes when compared to the other species described as tolerant to PeAfpC or chPeAFPV3.

Knowledge regarding the binding of AFPs to phospholipids is scarce. Here we have found that parental and chimeric AFPs, with the exception of PeAfpC, chPeAFPV2 and chPeAFPV3, bind to multiple phospholipids, but with higher affinity to phosphatidylinositol monophosphates. To the best of our knowledge, the only available example was reported by Lacadena et al. 1995 [61], who demonstrated that *A. giganteus* AFP was able to promote the aggregation of vesicles composed of a negatively charged synthetic phospholipid. Conversely, much more work has been done with antifungal plant defensins. Binding to membrane phospholipids has been described for several defensins such as NaD1 from *N. alata* [57], the tomato defensin TPP3 [62], or MtDef4 and MtDef5 from *Medicago truncatula* [63,64]. TTP3 has a unique lipid binding profile that is specific for PtdIns(4,5)P_2, whereas NaD1, MtDef4 and MtDef5 bind to several phospholipids. Similar to the AFPs and chimeras evaluated here, MtDef5 showed preference for phosphatidylinositol monophosphates, as compared to bi- and triphosphates [64]. It has been described that interaction of defensins with phospholipids leads to their oligomerization, and that this ability to self-assemble into oligomers is important for their antimicrobial activity [57,62,64]. Moreover, MtDef5 forms oligomers with a broad range of phospholipids independently of the binding affinity, and this has been related to its potent antifungal activity against a broad range of fungi [64]. We did not observe any oligomerization of PeAFPs or chimeras in the presence of PA (data not shown) to which the proteins show binding in the lipid-protein interaction assays. Whether AFP oligomerization is required for antifungal activity requires further studies. Attempts to co-crystallize PeAFPs and chimeras in the presence of membrane phospholipids are in progress.

Antifungals targeting the cell wall are promising weapons against antifungal resistance. Most fungal cell walls are composed of the inner layer comprising a relatively conserved structural skeleton of chitin and glucans, and the more heterogeneous outer layer which is composed of heavily mannosylated O- and N-glycoproteins [65]. The structure of these oligosaccharide side chains differs among fungal species [66]. The role of mannosylated glycoproteins in the interaction of antifungal peptides and proteins with fungi is well documented [67–70]. In previous studies we demonstrated that the gene coding for protein O-mannosyltransferase 2 (Pmt2), which is responsible for the addition of the first mannosyl residue of O-linked carbohydrates, determines the susceptibility of *S. cerevisiae* and *P. digitatum* to the hexapeptide PAF26 [37,71]. Recently, we described that PdAfpB interaction with the cell wall is important for its activity by facilitating access to the plasma membrane and subsequent entry into the fungal cell [15]. Moreover, we showed that the *P. digitatum* Δ*pmt2* mutant deficient in protein mannosylation also had increased tolerance to PdAfpB, in correlation with the absence of protein interaction and internalization observed by the confocal microscopy of Δ*pmt2* cells treated with the fluorescently labeled PdAfpB [15]. In accordance with these results, here we show that the Δ*pmt2* mutant had increased tolerance to parental and chimeric AFPs, suggesting the role of the mannoproteins surrounding the fungal cell in the mechanism of action. It is noteworthy that PeAfpA and the two chimeric proteins chPeAFPV1 and chPeAFPV2, the most active proteins against *P. digitatum* wt, affected to a greater or lesser extent the Δ*pmt2* mutant fungal growth suggesting that interaction with the cell wall is important but not essential for the antifungal activity. Based on its 3D structure, *A. giganteus* AFP was originally described as an oligonucleotide/oligosaccharide binding (OB) fold-containing protein [72]. Later on, immunogold electron microscopy showed that the *A. giganteus* AFP binds to the region rich in glycoproteins of the outer layer, as well as to the cell wall, of hyphal cells of the AFP-sensitive *A. niger* while very

little protein was bound to the outer layer and cell wall of AFP-resistant *P. chrysogenum* cells [73]. Interestingly, authors also described that in contrast to that observed in *A. niger* cells, glycoproteins were barely distributed on the cell wall surface of *P. chrysogenum*, and thus less AFP was detected there [73]. Whether the heterogeneity and species-specific peculiarities of the outer layer and specifically of the mannoproteins can explain the spectrum activity and mode of action of PeAFPs and chimeras requires further studies.

5. Conclusion

In summary, we have demonstrated that class A and B AFPs present a highly conserved structural scaffold. This structural conservation has allowed us to swap PeAfpB and PeAfpA sequences, generating chimeric AFPs with both improved and impaired antifungal activity and providing new insights about the relevance of sequence motifs. Our data also confirm that AFPs seem to have multiple cell targets that would explain the broad antifungal spectrum and selectivity. Combination of rational design with 3D structure suggests that specific differences in the amino acid sequence of the chimeras determine their antifungal activity and probably the mode of action, more than the overall fold or physicochemical properties. Future efforts are directed to an in-depth characterization of the mode of action of PeAfpA and the most interesting chimeras.

CRediT authorship contribution statement

Moisés Giner-Llorca: Investigation, Writing – original draft, Visualization. **Francisca Gallego del Sol:** Investigation, Writing – original draft, Visualization. **Jose F. Marcos:** Conceptualization, Writing – review & editing, Supervision, Project administration, Funding acquisition. **Alberto Marina:** Conceptualization, Writing – original draft, Writing – review & editing, Supervision, Project administration, Funding acquisition. **Paloma Manzanares:** Conceptualization, Writing – original draft, Writing – review & editing, Supervision, Project administration, Funding acquisition.

Declaration of competing interest

The authors declare that they have no known competing financial interests or personal relationships that could have appeared to influence the work reported in this paper.

Data availability

Coordinates and structure factors for PeAfpB, chPeAFPV1, chPeAFPV3, chPeAFPV4 and chPeAFPV5 have been deposited in the Protein Data Bank with access codes 7ZTF, 7ZUT, 7ZVH, 7ZW2 and 7ZTJ, respectively.

Acknowledgments

We would like to thank the IBV-CSIC Crystallogenesis Facility for protein crystallization screenings. The structural results reported in this article derive from measurements made at the synchrotron DLS (Didcot, UK), ALBA (Cerdanyola del Valles, Spain) and ESRF (Grenoble, France). Data collection experiments for the best crystals were carried at XALOC, I24 and ID23-2 beamlines at ALBA, DLS and ESRF Synchrotrons, respectively. X-ray diffraction data collection was supported by block allocation group (BAG) DLS Proposal MX28394, ALBA Proposal 2020074406 and ESRF proposal MX-2351. We acknowledge the ESRF, ALBA and DLS synchrotrons for provision of beam time and we would like to thank beamline staff for assistance. This work was supported by grants RTI2018-101115-B-C21, PID2021-125858OB-100 (to PM and JFM) and PID2019-108541GB-I00 (to AM) funded by MCIN/AEI/10.13039/501100011033 and by "ERDF A way of making Europe", and PROMETEO/2018/066 (to PM and JFM) and PROMETEO/2020/012 (to AM) by Valencian Government (Conselleria de Educación, Investigación, Cultura y Deporte). MGL was recipient of a predoctoral grant FPU19/02066 funded by MCIN/AEI/10.13039/501100011033 and by "ESF Investing in your future".

Appendix A. Supplementary data

Supplementary data to this article can be found online at https://doi.org/10.1016/j.ijbiomac.2022.11.280.

References

[1] J. Delgado, R.A. Owens, S. Doyle, M.A. Asensio, F. Núñez, Antifungal proteins from moulds: analytical tools and potential application to dry-ripened foods, Appl. Microbiol. Biotechnol. 100 (16) (2016) 6991–7000.
[2] N. Hegedüs, F. Marx, Antifungal proteins: more than antimicrobials? Fungal Biol. Rev. 26 (4) (2013) 132–145.
[3] P.V. Martínez-Culebras, M. Gandía, S. Garrigues, J.F. Marcos, P. Manzanares, Antifungal peptides and proteins to control toxigenic fungi and mycotoxin biosynthesis, Int. J. Mol. Sci. 22 (24) (2021) 13261.
[4] F. Marx, U. Binder, É. Leiter, I. Pócsi, The Penicillium chrysogenum antifungal protein PAF, a promising tool for the development of new antifungal therapies and fungal cell biology studies, Cell. Mol. Life Sci. 65 (3) (2008) 445–454.
[5] G. Batta, T. Barna, Z. Gáspári, S. Sándor, K.E. Kövér, U. Binder, B. Sarg, L. Kaiserer, A.K. Chhillar, A. Eigentler, É. Leiter, N. Hegedüs, I. Pócsi, H. Lindner, F. Marx, Functional aspects of the solution structure and dynamics of PAF – a highly-stable antifungal protein from Penicillium chrysogenum, FEBS J. 276 (10) (2009) 2875–2890.
[6] N.Y. Yount, M.R. Yeaman, Multidimensional signatures in antimicrobial peptides, Proc. Natl. Acad. Sci. U. S. A. 101 (19) (2004) 7363–7368.
[7] F. Marx, H. Haas, M. Reindl, G. Stöffler, F. Lottspeich, B. Redl, Cloning, structural organization and regulation of expression of the Penicillium chrysogenum paf gene encoding an abundantly secreted protein with antifungal activity, Gene 167 (1–2) (1995) 167–171.
[8] S. Garrigues, M. Gandía, J.F. Marcos, Occurrence and function of fungal antifungal proteins: a case study of the citrus postharvest pathogen Penicillium digitatum, Appl. Microbiol. Biotechnol. 100 (5) (2016) 2243–2256.
[9] M. Gandía, E. Moreno-Giménez, M. Giner-Llorca, S. Garrigues, C. Ropero-Pérez, A. Locascio, P.V. Martínez-Culebras, J.F. Marcos, P. Manzanares, Development of a FungalBraid (FB) Penicillium expansum-based expression system for the production of antifungal proteins (AFPs) in fungal biofactories, Microb. Biotechnol. 15 (2) (2022) 630–647.
[10] X. Shi, T. Cordero, S. Garrigues, J.F. Marcos, J.-A. Daròs, M. Coca, Efficient production of antifungal proteins in plants using a new transient expression vector derived from tobacco mosaic virus, Plant Biotechnol. J. 17 (6) (2019) 1069–1080.
[11] C. Sonderegger, L. Galgóczy, S. Garrigues, Á. Fizil, A. Borics, P. Manzanares, N. Hegedüs, A. Huber, J.F. Marcos, G. Batta, F. Marx, A Penicillium chrysogenum-based expression system for the production of small, cysteine-rich antifungal proteins for structural and functional analyses, Microb. Cell Factories 15 (1) (2016) 192.
[12] J. Holzknecht, A. Kühbacher, C. Papp, A. Farkas, G. Váradi, J.F. Marcos, P. Manzanares, G.K. Tóth, L. Galgóczy, F. Marx, The Penicillium chrysogenum Q176 antimicrobial protein PAFC effectively inhibits the growth of the opportunistic human pathogen Candida albicans, J. Fungi 6 (3) (2020) 141.
[13] A. Huber, D. Hajdu, D. Bratschun-Khan, Z. Gáspári, M. Varbanov, S. Philippot, Á. Fizil, A. Czajlik, Z. Kele, C. Sonderegger, L. Galgóczy, A. Bodor, F. Marx, G. Batta, New antimicrobial potential and structural properties of PAFB: a cationic, cysteine-rich protein from Penicillium chrysogenum Q176, Sci. Rep. 8 (1) (2018) 1751.
[14] É. Leiter, H. Szappanos, C. Oberparleiter, L. Kaiserer, L. Csernoch, T. Pusztahelyi, T. Emri, I. Pócsi, W. Salvenmoser, F. Marx, Antifungal protein PAF severely affects the integrity of the plasma membrane of Aspergillus nidulans and induces an apoptosis-like phenotype, Antimicrob. Agents Chemother. 49 (6) (2005) 2445.
[15] A. Bugeda, S. Garrigues, M. Gandía, P. Manzanares, J.F. Marcos, M. Coca, The antifungal protein AfpB induces regulated cell death in its parental fungus Penicillium digitatum, mSphere 5 (4) (2020), e00595-20.
[16] V. Meyer, A small protein that fights fungi: AFP as a new promising antifungal agent of biotechnological value, Appl. Microbiol. Biotechnol. 78 (1) (2008) 17–28.
[17] A.B. Moreno, A. Martínez Del Pozo, B. San Segundo, Biotechnologically relevant enzymes and proteins. Antifungal mechanism of the Aspergillus giganteus AFP against the rice blast fungus Magnaporthe grisea, Appl. Microbiol. Biotechnol. 72 (5) (2006) 883–895.
[18] N. Paege, D. Warnecke, S. Zäuner, S. Hagen, A. Rodrigues, B. Baumann, M. Thiess, S. Jung, V. Meyer, Species-specific differences in the susceptibility of fungi to the antifungal protein AFP depend on C-3 saturation of glycosylceramides, mSphere 4 (6) (2019), e00741-19.
[19] R. Kovács, J. Holzknecht, Z. Hargitai, C. Papp, A. Farkas, A. Borics, L. Tóth, G. Váradi, G.K. Tóth, I. Kovács, S. Dubrac, L. Majoros, F. Marx, L. Galgóczy, In vivo applicability of Neosartorya fischeri antifungal protein 2 (NFAP2) in treatment of vulvovaginal candidiasis, Antimicrob. Agents Chemother. 63 (2) (2019), e01777-18.

[20] M. Gandía, S. Garrigues, B. Bolós, P. Manzanares, J.F. Marcos, The myosin motor domain-containing chitin synthases are involved in cell wall integrity and sensitivity to antifungal proteins in Penicillium digitatum, Front. Microbiol. 10 (2400) (2019).
[21] S. Hagen, F. Marx, A.F. Ram, V. Meyer, The antifungal protein AFP from Aspergillus giganteus inhibits chitin synthesis in sensitive fungi, Appl. Environ. Microbiol. 73 (7) (2007) 2128–2134.
[22] A. Huber, G. Oemer, N. Malanovic, K. Lohner, L. Kovács, W. Salvenmoser, J. Zschocke, M.A. Keller, F. Marx, Membrane sphingolipids regulate the fitness and antifungal protein susceptibility of Neurospora crassa, Front. Microbiol. 10 (605) (2019).
[23] U. Binder, M. Bencina, A. Eigentler, V. Meyer, F. Marx, The Aspergillus giganteus antifungal protein AFP(NN5353) activates the cell wall integrity pathway and perturbs calcium homeostasis, BMC Microbiol. 11 (2011) 209.
[24] M. Gandía, S. Garrigues, M. Hernanz-Koers, P. Manzanares, J.F. Marcos, Differential roles, crosstalk and response to the antifungal protein AfpB in the three mitogen-activated protein kinases (MAPK) pathways of the citrus postharvest pathogen Penicillium digitatum, Fungal Genet. Biol. 124 (2019) 17–28.
[25] C. Sonderegger, Á. Fizil, L. Burtscher, D. Hajdu, A. Muñoz, Z. Gáspári, N.D. Read, G. Batta, F. Marx, D19S mutation of the cationic, cysteine-rich protein PAF: novel insights into its structural dynamics, thermal unfolding and antifungal function, PLOS ONE 12 (1) (2017), e0169920.
[26] C. Sonderegger, G. Váradi, L. Galgóczy, S. Kocsubé, W. Posch, A. Borics, S. Dubrac, G.K. Tóth, D. Wilflingseder, F. Marx, The evolutionary conserved γ-core motif influences the anti-Candida activity of the Penicillium chrysogenum antifungal protein PAF, Front. Microbiol. 9 (1655) (2018).
[27] L. Galgóczy, A. Borics, M. Virágh, H. Ficze, G. Váradi, Z. Kele, F. Marx, Structural determinants of Neosartorya fischeri antifungal protein (NFAP) for folding, stability and antifungal activity, Sci. Rep. 7 (1) (2017) 1963.
[28] S. Garrigues, M. Gandía, A. Borics, F. Marx, P. Manzanares, J.F. Marcos, Mapping and identification of antifungal peptides in the putative antifungal protein AfpB from the filamentous fungus Penicillium digitatum, Front. Microbiol. 8 (592) (2017).
[29] M. Heredero, S. Garrigues, M. Gandía, J.F. Marcos, P. Manzanares, Rational design and biotechnological production of novel AfpB-PAF26 chimeric antifungal proteins, Microorganisms 6 (4) (2018) 106.
[30] M. Gandia, A. Monge, S. Garrigues, H. Orozco, M. Giner-Llorca, J.F. Marcos, P. Manzanares, Novel insights in the production, activity and protective effect of Penicillium expansum antifungal proteins, Int. J. Biol. Macromol. 164 (2020) 3922–3931.
[31] S. Garrigues, M. Gandía, L. Castillo, M. Coca, F. Marx, J.F. Marcos, P. Manzanares, Three antifungal proteins from Penicillium expansum: different patterns of production and antifungal activity, Front. Microbiol. 9 (2370) (2018).
[32] P.V. Martínez-Culebras, M. Gandía, A. Boronat, J.F. Marcos, P. Manzanares, Differential susceptibility of mycotoxin-producing fungi to distinct antifungal proteins (AFPs), Food Microbiol. 97 (2021), 103760.
[33] N. Hegedüs, C. Sigl, I. Zadra, I. Pócsi, F. Marx, The paf gene product modulates asexual development in Penicillium chrysogenum, J. Basic Microbiol. 51 (3) (2011) 253–262.
[34] M. Hernanz-Koers, M. Gandía, S. Garrigues, P. Manzanares, L. Yenush, D. Orzaez, J.F. Marcos, FungalBraid: a GoldenBraid-based modular cloning platform for the assembly and exchange of DNA elements tailored to fungal synthetic biology, Fungal Genet. Biol. 116 (2018) 51–61.
[35] M. Vazquez-Vilar, M. Gandía, V. García-Carpintero, E. Marqués, A. Sarrion-Perdigones, L. Yenush, J. Polaina, P. Manzanares, J.F. Marcos, D. Orzaez, Multigene engineering by GoldenBraid cloning: from plants to filamentous fungi and beyond, Curr. Protoc. Mol. Biol. 130 (1) (2020), e116.
[36] M. Gandía, E. Harries, J.F. Marcos, The myosin motor domain-containing chitin synthase PdChsVII is required for development, cell wall integrity and virulence in the citrus postharvest pathogen Penicillium digitatum, Fungal Genet. Biol. 67 (2014) 58–70.
[37] E. Harries, M. Gandía, L. Carmona, J.F. Marcos, The Penicillium digitatum protein O-mannosyltransferase Pmt2 is required for cell wall integrity, conidiogenesis, virulence and sensitivity to the antifungal peptide PAF26, Mol. Plant Pathol. 16 (7) (2015) 748–761.
[38] C.H. Khang, S.Y. Park, H.S. Rho, Y.H. Lee, S. Kang, Filamentous fungi (Magnaporthe grisea and Fusarium oxysporum), Methods Mol. Biol. 344 (2006) 403–420.
[39] U.K. Laemmli, Cleavage of structural proteins during the assembly of the head of bacteriophage T4, Nature 227 (5259) (1970) 680–685.
[40] W. Kabsch, XDS, Acta Crystallogr. D Biol. Crystallogr. 66 (Pt 2) (2010) 125–132.
[41] P. Evans, Scaling and assessment of data quality, Acta Crystallogr. D Biol. Crystallogr. 62 (Pt 1) (2006) 72–82.
[42] A. Vagin, A. Teplyakov, Molecular replacement with MOLREP, Acta Crystallogr. D Biol. Crystallogr. 66 (Pt 1) (2010) 22–25.
[43] P. Emsley, K. Cowtan, Coot: model-building tools for molecular graphics, Acta Crystallogr. D Biol. Crystallogr. 60 (Pt 12 Pt 1) (2004) 2126–2132.
[44] A.A. Vagin, R.A. Steiner, A.A. Lebedev, L. Potterton, S. McNicholas, F. Long, G. N. Murshudov, REFMAC5 dictionary: organization of prior chemical knowledge and guidelines for its use, Acta Crystallogr. D Biol. Crystallogr. 60 (Pt 12 Pt 1) (2004) 2184–2195.
[45] E. Jurrus, D. Engel, K. Star, K. Monson, J. Brandi, L.E. Felberg, D.H. Brookes, L. Wilson, J. Chen, K. Liles, M. Chun, P. Li, D.W. Gohara, T. Dolinsky, R. Konecny, D.R. Koes, J.E. Nielsen, T. Head-Gordon, W. Geng, R. Krasny, G.-W. Wei, M. J. Holst, J.A. McCammon, N.A. Baker, Improvements to the APBS biomolecular solvation software suite, Protein Sci. 27 (1) (2018) 112–128.
[46] F. Guagnini, A. Huber, J.M. Alex, F. Marx, P.B. Crowley, Porous assembly of an antifungal protein mediated by zinc and sulfonato-calix[8]arene, J. Struct. Biol. 213 (2) (2021), 107711.
[47] R. Campos-Olivas, M. Bruix, J. Santoro, J. Lacadena, A. Martinez del Pozo, J. G. Gavilanes, M. Rico, NMR solution structure of the antifungal protein from Aspergillus giganteus: evidence for cysteine pairing isomerism, Biochemistry 34 (9) (1995) 3009–3021.
[48] D. Hajdu, A. Huber, A. Czajlik, L. Tóth, Z. Kele, S. Kocsubé, Á. Fizil, F. Marx, L. Galgóczy, G. Batta, Solution structure and novel insights into phylogeny and mode of action of the Neosartorya (Aspergillus) fischeri antifungal protein (NFAP), Int. J. Biol. Macromol. 129 (2019) 511–522.
[49] J.M. Alex, M.L. Rennie, S. Engilberge, G. Lehoczki, H. Dorottya, A. Fizil, G. Batta, P. B. Crowley, Calixarene-mediated assembly of a small antifungal protein, IUCrJ 6 (2) (2019) 238–247.
[50] J.G. Olsen, C. Flensburg, O. Olsen, G. Bricogne, A. Henriksen, Solving the structure of the bubble protein using the anomalous sulfur signal from single-crystal in-house Cu K[alpha] diffraction data only, Acta Crystallogr. D 60 (2) (2004) 250–255.
[51] A. Czajlik, J. Holzknecht, L. Galgóczy, L. Tóth, P. Poór, A. Ördög, G. Váradi, A. Kühbacher, A. Borics, G.K. Tóth, F. Marx, G. Batta, Solution structure, dynamics, and new antifungal aspects of the cysteine-rich miniprotein PAFC, Int. J. Mol. Sci. 22 (3) (2021) 1183.
[52] E. Krissinel, K. Henrick, Secondary-structure matching (SSM), a new tool for fast protein structure alignment in three dimensions, Acta Crystallogr. D 60 (12 Part 1) (2004) 2256–2268.
[53] J. Jumper, R. Evans, A. Pritzel, T. Green, M. Figurnov, O. Ronneberger, K. Tunyasuvunakool, R. Bates, A. Žídek, A. Potapenko, A. Bridgland, C. Meyer, S.A. A. Kohl, A.J. Ballard, A. Cowie, B. Romera-Paredes, S. Nikolov, R. Jain, J. Adler, T. Back, S. Petersen, D. Reiman, E. Clancy, M. Zielinski, M. Steinegger, M. Pacholska, T. Berghammer, S. Bodenstein, D. Silver, O. Vinyals, A.W. Senior, K. Kavukcuoglu, P. Kohli, D. Hassabis, Highly accurate protein structure prediction with AlphaFold, Nature 596 (7873) (2021) 583–589.
[54] S. Garrigues, M. Gandía, C. Popa, A. Borics, F. Marx, M. Coca, J.F. Marcos, P. Manzanares, Efficient production and characterization of the novel and highly active antifungal protein AfpB from Penicillium digitatum, Sci. Rep. 7 (1) (2017) 14663.
[55] L. Tóth, G. Váradi, A. Borics, G. Batta, Z. Kele, Á. Vendrinszky, R. Tóth, H. Ficze, G. K. Tóth, C. Vágvölgyi, F. Marx, L. Galgóczy, Anti-candidal activity and functional mapping of recombinant and synthetic Neosartorya fischeri antifungal protein 2 (NFAP2), Front. Microbiol. 9 (393) (2018).
[56] B. Lopez-García, E. Perez-Payá, J.F. Marcos, Identification of novel hexapeptides bioactive against phytopathogenic fungi through screening of a synthetic peptide combinatorial library, Appl. Environ. Microbiol. 68 (5) (2002) 2453–2460.
[57] I.K.H. Poon, A.A. Baxter, F.T. Lay, G.D. Mills, C.G. Adda, J.A.E. Payne, T.K. Phan, G.F. Ryan, J.A. White, P.K. Veneer, N.L. van der Weerden, M.A. Anderson, M. Kvansakul, M.D. Hulett, Phosphoinositide-mediated oligomerization of a defensin induces cell lysis, eLife 3 (2014), e01808.
[58] U.S. Sagaram, R. Pandurangi, J. Kaur, T.J. Smith, D.M. Shah, Structure-activity determinants in antifungal plant defensins MsDef1 and MtDef4 with different modes of action against Fusarium graminearum, PLOS ONE 6 (4) (2011), e18550.
[59] A. Huber, L. Galgóczy, G. Váradi, J. Holzknecht, A. Kakar, N. Malanovic, R. Leber, J. Koch, M.A. Keller, G. Batta, G.K. Tóth, F. Marx, Two small, cysteine-rich and cationic antifungal proteins from Penicillium chrysogenum: a comparative study of PAF and PAFB, Biochim. Biophys. ActaBiomembr. 1862 (8) (2020), 183246.
[60] M.R. Bleackley, J.A. Payne, B.M. Hayes, T. Durek, D.J. Craik, T.M. Shafee, I. K. Poon, M.D. Hulett, N.L. van der Weerden, M.A. Anderson, Nicotiana alata defensin chimeras reveal differences in the mechanism of fungal and tumor cell killing and an enhanced antifungal variant, Antimicrob. Agents Chemother. 60 (10) (2016) 6302–6312.
[61] J. Lacadena, A. Martínez del Pozo, M. Gasset, B. Patiño, R. Campos-Olivas, C. Vázquez, A. Martínez-Ruiz, J.M. Mancheño, M. Oñaderra, J.G. Gavilanes, Characterization of the antifungal protein secreted by the mould Aspergillus giganteus, Arch. Biochem. Biophys 324 (2) (1995) 273–281.
[62] A.A. Baxter, V. Richter, F.T. Lay, I.K. Poon, C.G. Adda, P.K. Veneer, T.K. Phan, M. R. Bleackley, M.A. Anderson, M. Kvansakul, M.D. Hulett, The tomato defensin TPP3 binds phosphatidylinositol (4,5)-bisphosphate via a conserved dimeric cationic grip conformation to mediate cell lysis, Mol. Cell. Biol. 35 (11) (2015) 1964–1978.
[63] K. El-Mounadi, K.T. Islam, P. Hernández-Ortiz, N.D. Read, D.M. Shah, Antifungal mechanisms of a plant defensin MtDef4 are not conserved between the ascomycete fungi Neurospora crassa and Fusarium graminearum, Mol. Microbiol. 100 (3) (2016) 542–559.
[64] K.T. Islam, S.L.S. Velivelli, R.H. Berg, B. Oakley, D.M. Shah, A novel bi-domain plant defensin MtDef5 with potent broad-spectrum antifungal activity binds to multiple phospholipids and forms oligomers, Sci. Rep. 7 (1) (2017) 16157.
[65] S.L. Lima, A.L. Colombo, J.N. de Almeida Junior, Fungal cell wall: emerging antifungals and drug resistance, Front. Microbiol. 10 (2573) (2019).
[66] N.A.R. Gow, J.P. Latge, C.A. Munro, The fungal cell wall: structure, biosynthesis, and function, Microbiol. Spectr. 5 (3) (2017).
[67] M. Gentzsch, W. Tanner, The PMT gene family: protein O-glycosylation in Saccharomyces cerevisiae is vital, EMBO J. 15 (21) (1996) 5752–5759.
[68] M. Harris, H.M. Mora-Montes, N.A.R. Gow, P.J. Coote, Loss of mannosylphosphate from Candida albicans cell wall proteins results in enhanced resistance to the inhibitory effect of a cationic antimicrobial peptide via reduced peptide binding to the cell surface, Microbiology 155 (Pt 4) (2009) 1058–1070.

[69] J.I. Ibeas, H. Lee, B. Damsz, D.T. Prasad, J.M. Pardo, P.M. Hasegawa, R.A. Bressan, M.L. Narasimhan, Fungal cell wall phosphomannans facilitate the toxic activity of a plant PR-5 protein, Plant J. 23 (3) (2000) 375–383.
[70] E. Szafranski-Schneider, M. Swidergall, F. Cottier, D. Tielker, E. Román, J. Pla, J. F. Ernst, Msb2 shedding protects Candida albicans against antimicrobial peptides, PLoS Pathog. 8 (2) (2012), e1002501.
[71] E. Harries, L. Carmona, A. Muñoz, J.I. Ibeas, N.D. Read, M. Gandía, J.F. Marcos, Genes involved in protein glycosylation determine the activity and cell internalization of the antifungal peptide PAF26 in Saccharomyces cerevisiae, Fungal Genet. Biol. 58–59 (2013) 105–115.
[72] Á. Martínez del Pozo, V. Lacadena, J.M. Mancheño, N. Olmo, M. Oñaderra, J. G. Gavilanes, The antifungal protein AFP of Aspergillus giganteus is an oligonucleotide/oligosaccharide binding (OB) fold-containing protein that produces condensation of DNA, J. Biol. Chem. 277 (48) (2002) 46179–46183.
[73] T. Theis, F. Marx, W. Salvenmoser, U. Stahl, V. Meyer, New insights into the target site and mode of action of the antifungal protein of Aspergillus giganteus, Res. Microbiol. 156 (1) (2005) 47–56.
[74] E. Gasteiger, C. Hoogland, A. Gattiker, S.e. Duvaud, M.R. Wilkins, R.D. Appel, A. Bairoch, Protein identification and analysis tools on the ExPASy server, in: J. M. Walker (Ed.), The Proteomics Protocols Handbook, Humana Press, Totowa, NJ, 2005, pp. 571–607.